Microelectronics Journal

Enhancement in Analog/RF and Power Performance of Underlapped Quaternary DG GaN/InAlGaN MOSHEMTs

--Manuscript Draft--

Manuscript Number:	
Article Type:	Research Paper
Keywords:	Analog, Double Gate, InAlGaN/GaN, MOS-HEMT, RF, Power, Symmetric Underlap
Corresponding Author:	Atanu Kundu Heritage Institute of Technology Kolkata, India
First Author:	Hrit Mukherjee, Undergraduate Student
Order of Authors:	Hrit Mukherjee, Undergraduate Student
	Mousiki Kar, Ph.D (Engg.)
	Atanu Kundu, Ph.D. (Engg.)
Abstract:	In this paper, an U-DG quaternary In 0.05 Al 0.75 Ga 0.2 N/GaN based MOS-HEMT and a conventional ternary Al 0.3 Ga 0.7 N/GaN based MOS-HEMT of same device structure have been analyzed and compared by investigating their Analog, RF and Power performances. Quaternary InAlGaN heterostructure experiences almost 3 times 2DEG concentration and thus showcases 171.8% higher saturation drain current density (Id), than ternary AlGaN. The influence of InAlGaN layer has also been studied by varying barrier thickness and 10.8% higher f T and 9.1% higher f MAX values of InAlGaN MOS-HEMT with respect to AlGaN MOS-HEMT, of same barrier width, proves the former's predominance in building high frequency amplifiers. These percentages raise upto 18.3% and 54.6% respectively for thinner quaternary barrier width of 7nm. Large signal analysis for 7nm InAlGaN/GaN MOS-HEMT at 100 GHz records a higher gain with 87.5% output power efficiency compared to 42.5% of 18nm AlGaN/GaN MOS-HEMT at same input of 45 dBm.

From,

Atanu Kundu

Heritage Institute of Technology

Kolkata-700107

West Bengal, India

To,

The Editor,

Microelectronics Journal,

Respected Sir/ Madam,

This is to inform you that we are submitting our manuscript entitled "**Enhancement in Analog/RF and Power Performance of Underlapped Quaternary DG GaN/InAlGaN MOSHEMTs**" for possible publication in the **Microelectronics Journal**.

Title: Enhancement in Analog/RF and Power Performance of Underlapped Quaternary DG GaN/InAlGaN MOSHEMTs.

Authors: Hrit Mukherjee, Mousiki Kar and Atanu Kundu

Kindly acknowledge the receipt of the same.

With Regards,

Atanu Kundu.

Highlights

- **Impact of Underlap on Quaternary GaN/InAlGaN DG-MOSHEMTs**
- **Subthreshold Analog/RF and Power Performance of Underlap on DG-MOSHEMTs**
- **Extraction of AC small signal parameters of Quaternary GaN/InAlGaN DG-MOSHEMTs**
- **RF parameters extraction using the Non Quasi Static (NQS) model of Quaternary GaN/InAlGaN DG-MOSHEMTs**
- **Large signal analysis of Quaternary GaN/InAlGaN DG-MOSHEMTs**

Enhancement in Analog/RF and Power Performance of Underlapped Quaternary DG GaN/InAlGaN MOSHEMTs

Hrit Mukherjee[a], Mousiki Kar[b] and Atanu Kundu[b*]

[a]*Department of Electronics and Tele-Communications Engineering, Jadavpur University, Kolkata, India*
[b]*Department of Electronics and Communications Engineering, Heritage Institute of Technology, Kolkata, India*

***Abstract*— In this paper, an U-DG quaternary $In_{0.05}Al_{0.75}Ga_{0.2}N$/GaN based MOS-HEMT and a conventional ternary $Al_{0.3}Ga_{0.7}N$/GaN based MOS-HEMT of same device structure have been analyzed and compared by investigating their Analog, RF and Power performances. Quaternary InAlGaN heterostructure having higher polarization charge density, experiences almost 3 times 2DEG concentration and thus showcases 171.8 % higher saturation drain current density (I_d), than ternary AlGaN having equal barrier width of 18 nm, at same working voltage of 1 V, validating improved Analog Performances. The influence of InAlGaN layer has also been studied for all performances by varying barrier thickness for 3 different widths, 18 nm, 13 nm and 7 nm. 10.8 % higher f_T and 9.1 % higher f_{MAX} values of InAlGaN MOS-HEMT with respect to AlGaN MOS-HEMT, of same barrier width of 18 nm, proves the former's predominance in building high frequency amplifiers. These percentages raise upto 18.3 % and 54.6 % respectively for thinner quaternary barrier width of 7 nm. Large signal analysis for 7 nm InAlGaN/GaN MOS-HEMT at 100 GHz records a higher gain with 87.5 % output power efficiency compared to 42.5 % of 18 nm AlGaN/GaN MOS-HEMT at same input of 45 dBm, eventually proving thin barrier quaternary MOS-HEMTs as a better candidate for sophisticated high power devices.**

***Index Terms*—Analog, Double Gate, InAlGaN/GaN, MOS-HEMT, RF, Power, Symmetric Underlap.**

I. Introduction

Modern GaN HEMTs have outclassed traditional Si MOSFETs owing to the former's improved performances in high frequency and high power applications. The chief disadvantage in using Si MOSFET in short channel devices is the degradation in its carrier mobility and thus, output current density owing to various short channel effects (SCEs), especially impurity scattering in the conducting channel. The non-uniform dopant distribution and dopant scattering in the channel, on application of sufficient gate voltage causes hindrance in the migration of carriers from source to drain, thereby reducing carrier mobility, drain current density and thus, output power density. Previous researches have proposed an alternative solution to this problem by replacing conventional MOSFETs by today's HEMT devices **[1]**. In AlGaN/GaN based HEMT devices, a two dimensional triangular potential well of electron gas is formed at the straddling heterojunction interface of AlGaN and GaN. Much higher carrier mobility and density is obtained which contributes to larger output current density without the inclusion of dopants in the undoped barrier region **[2]**. $Al_xGa_{1-x}N$/GaN HEMTs also show excellent material properties like wide and tunable bandgap, high breakdown voltage, high average electron drift velocity and good thermal conductivity **[3]**. Strained $Al_xGa_{1-x}N$/GaN HEMTs are capable of enhancing carrier density in the quantum well for its high piezoelectric polarization charge **[4]**.

Out of the two prevalent HEMT devices, namely Schottky-HEMTs and MOS-HEMTs, Schottky-HEMT is disadvantageous owing to its high gate leakage current which causes heating and power loss, undesirable for its use in low noise and high power appliances. Therefore, MOS-HEMT has emerged as the more promising alternative because of its higher input impedance and lower leakage current due to the presence of a high k dielectric oxide layer acting as the insulator between the gate and the channel. MOS-HEMTs are also advantageous over Schottky by virtue of its lower threshold voltage and higher drive current capacity due to greater amount of charge stored per unit length in its channel, thus yielding better analog performance **[5-6]**.

Gallium Nitride (GaN) and related III-V materials offer the promise of exceptional levels of performance for high-power, high-frequency applications, as well as for power conversion/control, radio astronomy, space, military applications, and entertainment applications in satellite broadcasting receivers, cryogenic low-noise systems, and radio telescope to detect microwave signals from a dark nebula, broadcasting satellite receivers, cell-phone handsets and automotive radars. The high-performance GaN-based devices for RF through mm-wave applications, as well as for power conversion and control are proposed in SOC, and novel advanced processing techniques promise to enable these devices to be heterogeneously integrated with Si and advanced packages while retaining the unsurpassed performance

* Corresponding author.
*E-mail address:*e-mail: kundu.atanu@gmail.com (A Kundu)

possible with GaN **[7]**. The maximum output power of a device is mainly governed by two factors, the maximum drain current density and the breakdown voltage. Hence, in order to upgrade the output power density at same working voltage, the drain current as well as the breakdown voltage must be increased. Increasing Al composition in the AlGaN barrier layer raises the bandgap energy and breakdown voltage of AlGaN, thereby creating greater conduction band energy difference between AlGaN and GaN. Thus 2DEG concentration, carrier mobility and drain current density increases, ultimately leading to better analog performance. Increased Al composition also reduces critical barrier thickness of AlGaN layer, thereby enhancing its radio frequency performances, too **[8]**.

However, uncontrolled growth of Al in AlGaN layer or directly using AlN interlayer cannot be entertained as the tensile stress aroused due to lattice mismatch between AlGaN and GaN severely deteriorates the crystal quality of heterostructures **[9]**.

Fortunately, In is found to be advantageous over Al in this respect. Replacing AlGaN by an InAlN layer with 18 % In is lattice matched to GaN and provides very high spontaneous polarization and almost double 2DEG values with respect to the former **[10-11]**.

Yet, high quality ternary InAlN is difficult to grow because of its immiscibility, phase separation and composition non-homogeneity, as reports suggest the presence of pits in the InAlN film corresponding to the dislocation defects in the GaN buffer and eventually leading to significantly high surface roughness **[12]**.

Auspiciously, quaternary InAlGaN promises to be a propitious barrier material providing high electron sheet density in the quantum well, as well as proving to be much more miscible, nullifying the above mentioned problems **[13]**. Quaternary InAlGaN having considerably higher bandgap than ternary AlGaN delivers higher breakdown voltage, further facilitating its predominance in high frequency and high power electronics **[14-16]**. Therefore, if In and Al mole fraction is appropriately modulated, very high quality HEMT devices can be fabricated **[17]**.

In this work, InAlGaN/GaN has been established as a better candidate with respect to conventional AlGaN/GaN in MOS-HEMT devices for high frequency and high power applications by studying their Analog, RF and Power performances. Increasing quaternary barrier width increases its 2DEG values by enhancing both its spontaneous and piezoelectric polarization charge, improving device's drain current density **[18]**. On the other hand, reducing barrier thickness strengthens gate control over the channel, making the device highly sensitive with a notable rise in the high frequency input power swing as it turns ON **[19]**. Hence, the device's performance has also been analyzed by modulating quaternary InAlGaN layer thickness in its optimal range **[20-22]**. A symmetric underlap has been employed on both sides of gate, i.e. the source side as well as the drain side, to create a physical isolation between the drain and gate, thereby suppressing DIBL and reducing I_{off} **[23]**. Double gates have been employed to attain better gate control over the channel and minimize SCEs **[24]**.

II. Device Structure and Simulation Procedure

The 2D cross sectional views of an U-DG GaN based heterostructured MOS-HEMT with ternary AlGaN and quaternary InAlGaN as barrier materials are depicted in **Fig.1** and **Fig.2** respectively. Molybdenum is one of the most conductive refractory metals and is chosen as the gate material as it provides significantly reduced gate resistance and forms a stable contact with the oxide layer at elevated temperatures. High k dielectric HfO_2 is used as the oxide material **[25-26]**. The metallic source and drain provides a work function of 4.31 eV. GaN being highly expensive, GaN HEMTs are usually fabricated on foreign substrates like sapphire, SiC and Si compounds **[27]**. Here, much more economic Si_3N_4 is used as the substrate material. As the optimal I_{on}/I_{off} ratio is recorded for channel thickness in the range 140-180 nm **[28]**, the GaN buffer thickness is chosen as 180 nm.

TABLE I
DEVICE PARAMETERS AND DIMENSIONS

Device Parameters	**Dimension**
Soucre/Drain Length (S)	200 nm
Gate Length (L_g)	200 nm
Source Underlap (L_s)	200 nm
Drain Underlap (L_d)	200 nm
Gate Height (g_h)	50 nm
Oxide thickness (t_{ox})	10 nm
Channel/buffer thickness (buf)	180 nm

Speculating the effects of polarization and mechanism of electron transfer at the AlGaN/GaN heterojunction, it can be concluded that for Al mole fraction 0.3, the density of the 2DEG is almost nil for thinnest AlGaN barrier (d = 3 nm), rises with increasing AlGaN width and saturates at near about d = 25 nm **[2]**. Therefore, d = 18 nm is chosen as the barrier thickness for comparing performances of ternary AlGaN and quaternary InAlGaN materials. Also, for the same reason, analysis of quaternary $In_{0.05}Al_{0.75}Ga_{0.2}N$/GaN MOS-HEMT by varying barrier width is done at d = 18 nm, 13 nm and 7 nm, where 2DEG concentration varies significantly.

All the simulations have been performed using TCAD device simulator on 1 µm fabrication technology. The model specifications that have been incorporated into the experimental prototype of the simulator are Shockley Read Hall recombination model, mobility model, Newton model, Fermi-Dirac statistics model, Albrecht model and polarization model. Shockley Read Hall recombination model is used to correctly estimate the active carrier lifetime. Mobility models are included to handle the effects of carrier mobility degradation due to SCEs **[29]**. Newton model provides convergent solution for root computations and Fermi-Dirac statistics model is used for consistent device simulations. Albrecht model is added to simulate low field mobility calibration and polarization model is used for polar GaN devices. The following section describes the performances of each device in detail.

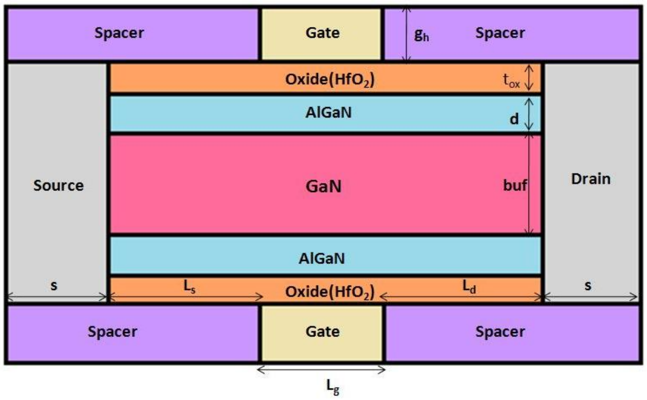

Fig. 1. Cross-sectional view of U-DG AlGaN/GaN MOS-HEMT structure.

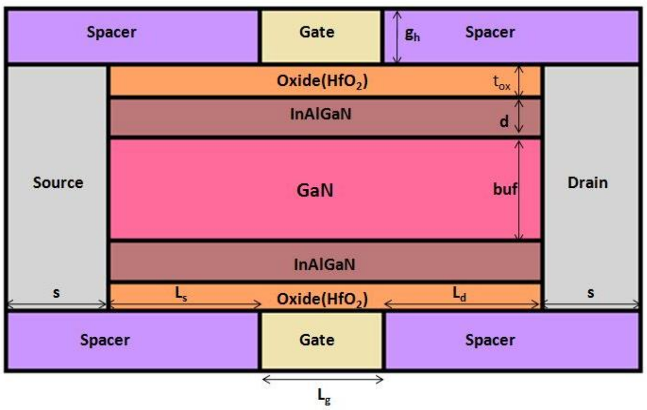

Fig. 2. Cross-sectional view of U-DG InAlGaN/GaN MOS-HEMT structure.

III. Analog Performance

The Analog FoMs that have been compared between the above mentioned ternary AlGaN/GaN and quaternary InAlGaN/GaN heterostructures include the variation of drain current density (I_d), transconductance (g_m), transconductance generation factor (g_m/I_d), output resistance (r_o) and intrinsic gain ($g_m r_o$). Each of these parameters has also been analyzed by varying barrier thickness of the InAlGaN/GaN based MOS-HEMT.

Electrical polarization has a substantial impact on the 2DEG concentration and the electric field distribution in heterojunction compounds. The quaternary InAlGaN barrier experiences a greater polarization induced sheet charge density in comparison to its ternary counterpart, majority of which comes from spontaneous polarization **[30]**. $In_yAl_xGa_zN$ provides an extra degree of freedom of bandgap mole fraction ratio compared to Al_xGa_zN, where x+y+z=1 in the former and x+z=1 in the latter.

$$P_{sp}(Al_xIn_yGa_zN) = x\cdot P_{sp}(AlN) + y\cdot P_{sp}(InN) + z\cdot P_{sp}(GaN) + b_{AlGaN}\cdot x\cdot z + b_{InGaN}\cdot y\cdot z + b_{AlInN}\cdot x\cdot y \quad \ldots(1)$$

$$P_{sp}(Al_xGa_zN) = x\cdot P_{sp}(AlN) + z\cdot P_{sp}(GaN) + b_{AlGaN}\cdot x\cdot z \quad \ldots(2)$$

$$P_{pz}(Al_xIn_yGa_zN) = x\cdot P_{pz}(AlN,\eta) + y\cdot P_{pz}(InN,\eta) + z\cdot P_{pz}(GaN,\eta) \quad \ldots(3)$$

$$P_{pz}(Al_xGa_zN) = x\cdot P_{pz}(AlN,\eta) + z\cdot P_{pz}(GaN,\eta) \quad \ldots(4)$$

From the expressions of piezoelectric polarization in (3) and (4), it is evident that the basal strain, η(x,y,z) of the respective barrier alloys is involved in the calculation of non-linear piezoelectric polarization of every binary component in the alloy, which is why it is also called strain-induced polarization. The charge density, σ_{int} at the heterojunction interface as indicated in (5) and (6) are manifested as the difference between P(barrier material) and P(buffer material), where P represents the total polarization of an alloy expressed as a sum of P_{sp} and P_{pz}.

$$\begin{aligned}\sigma_{\text{int}}(InAlGaN) &= P(GaN) - P(InAlGaN)\\ &= P_{sp}(GaN) - P_{sp}(InAlGaN) - P_{pz}(InAlGaN)\end{aligned} \quad \ldots(5)$$

$$\begin{aligned}\sigma_{\text{int}}(AlGaN) &= P(GaN) - P(AlGaN)\\ &= P_{sp}(GaN) - P_{sp}(AlGaN) - P_{pz}(AlGaN)\end{aligned} \quad \ldots(6)$$

Assuming barrier height, φ_B has already been predetermined, the electron density of the respective MOS-HEMTs are evaluated using (7) and (8), where d is the barrier thickness, Δ_{CB} is the conduction band energy discontinuity and Δ is the depth of band bending below the Fermi-level.

$$n_s(InAlGaN) = \frac{\sigma_{\text{int}}(InAlGaN)}{e} - \frac{\varepsilon_0\varepsilon_r\left[e\phi_b - \Delta + \Delta_{CB}\right]}{e^2 d} \quad \ldots(7)$$

$$n_s(AlGaN) = \frac{\sigma_{\text{int}}(AlGaN)}{e} - \frac{\varepsilon_0\varepsilon_r\left[e\phi_b - \Delta + \Delta_{CB}\right]}{e^2 d} \quad \ldots(8)$$

From (1) and (2), it can be concluded that InAlGaN based MOS-HEMT showcases greater P_{sp} due to the extra terms corresponding to InN in the former. Moreover, In being lattice matched to GaN experiences less strain and thus, controlled strain-induced polarization (P_{pz}), eventually establishing quaternary MOS-HEMT as the more stable heterostructure.

All these factors show that quaternary HEMT possesses an enormous polarization discontinuity between InAlGaN barrier and GaN channel, ultimately causing more band bending and higher sheet charge density. This significantly reduces the sheet resistance and uplifts the 2DEG concentration, as are evident from the values computed in the central part of the channel listed in the Table.II.

Fig.3 and **Fig.4** shows the variation of conduction band energy along the channel in OFF state for ternary and quaternary MOS-HEMTs and for various optimal barrier thicknesses respectively. **Fig.3** concludes that quaternary HEMT having lower OFF state conduction band energy than ternary will have greater device current despite showcasing

TABLE II

Parameters	$Al_{0.3}Ga_{0.7}N$	$In_{0.05}Al_{0.75}Ga_{0.2}N$	$In_{0.05}Al_{0.75}Ga_{0.2}N$	$In_{0.05}Al_{0.75}Ga_{0.2}N$
Barrier Width (nm)	18	18	13	7
Bandgap energy (eV)	3.972	4.965	4.965	4.965
GaN conduction band bending below Fermi level (eV)	0.187	0.396	0.390	0.376
Sheet charge density (σ_{int}) (C/cm^2)	1.56×10^{-6}	4.16×10^{-6}	4.16×10^{-6}	4.16×10^{-6}
2DEG concentration (n_s) (cm^{-2})	7.743×10^{12}	2.083×10^{13}	1.892×10^{13}	1.789×10^{13}

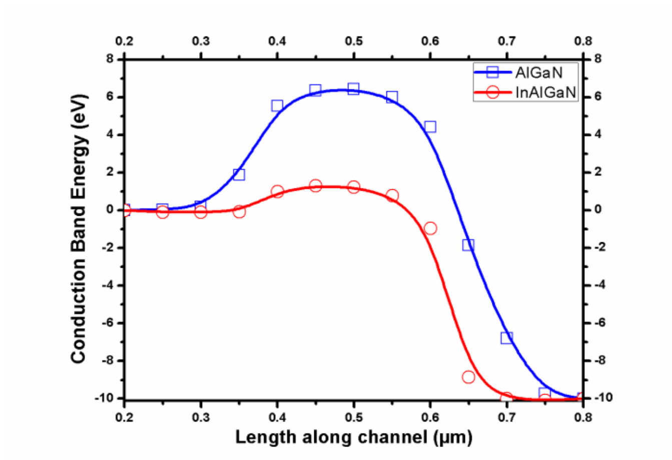

Fig. 3. Conduction Band Energy variation along the channel of U-DG GaN HEMT for 18 nm AlGaN and InAlGaN barrier widths at V_{ds} = 10V and V_{gs} = -10 V (OFF state).

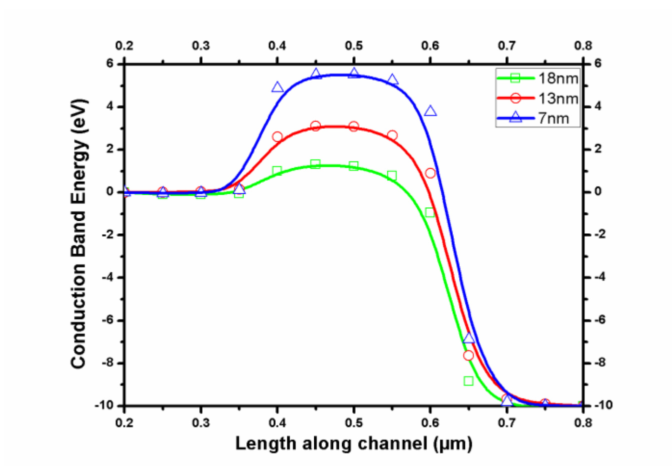

Fig. 4. Conduction Band Energy variation along the channel of U-DG InAlGaN/GaN HEMT for varying barrier widths at V_{ds} = 10V and V_{gs} = -10 V (OFF state).

more DIBL. Decreasing InAlGaN width enhances gate controllability over the conduction channel. Therefore, impact of gate on a MOS-HEMT having lower InAlGaN width is more than that having higher InAlGaN width. Hence, the MOS-HEMT with InAlGaN width 7nm, experiences least DIBL with respect to the other two, as is evident from its highest peak non-equilibrium potential barrier in OFF state as shown in **Fig.4**.

From the 2DEG concentration values cited in Table.II**,** it can be inferred that band bending and barrier lowering is more in InAlGaN MOS-HEMT at same working voltage which is in line with the conduction band energy variation along the channel in ON state shown in **Fig.5**. So, more number of carriers can overcome the potential barrier between source and drain, and traverse from source to drain, thereby leading to flow of higher conventional drain current in the opposite direction as is evident from I_d-V_{ds} variation, as shown is **Fig.6**.

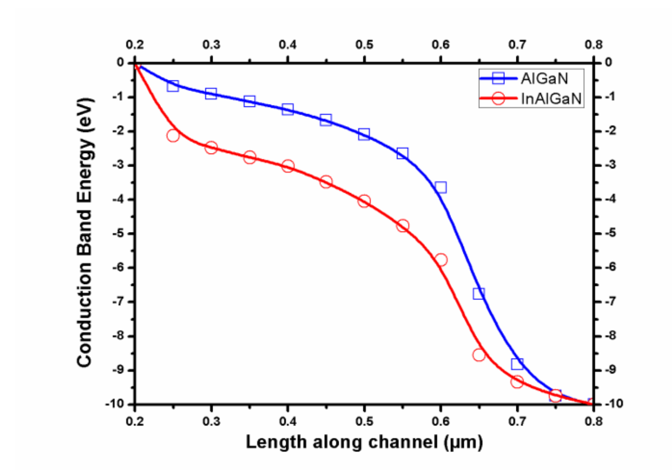

Fig. 5. Conduction Band Energy variation along the channel of U-DG GaN HEMT for 18 nm AlGaN and InAlGaN barrier widths at V_{ds} = 10V and V_{gs} = -10 V (OFF state).

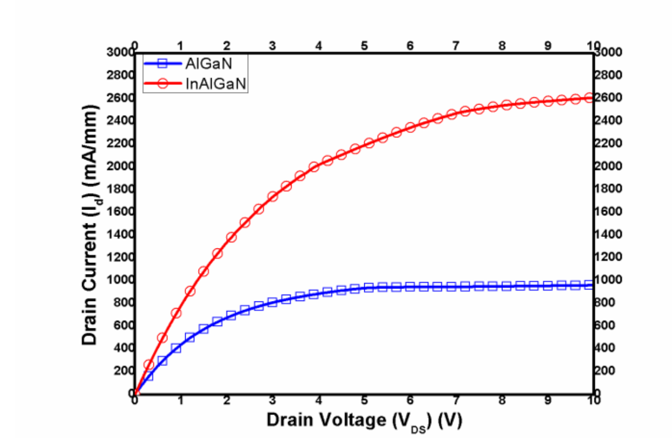

Fig. 6. Variation of I_d with V_{ds} of U-DG GaN HEMT for 18 nm InAlGaN and AlGaN barrier widths at V_{gs} = 1V.

Speculating the conduction band energy variations of **Fig.7**, it is evident that for the same reason the InAlGaN MOS-HEMT of width 18nm has the lowest barrier in OFF state, and on application of equal amount of bias on all the three specimens, it gets lowered to the largest extent in ON state. Hence, increased electron sheet concentration in the channel as a result of increasing barrier thickness causes comparatively more conduction band lowering. This increased band bending and thus, carrier mobility with increasing barrier width contributes to larger drain current variations with drain voltage, as depicted in **Fig.8**.

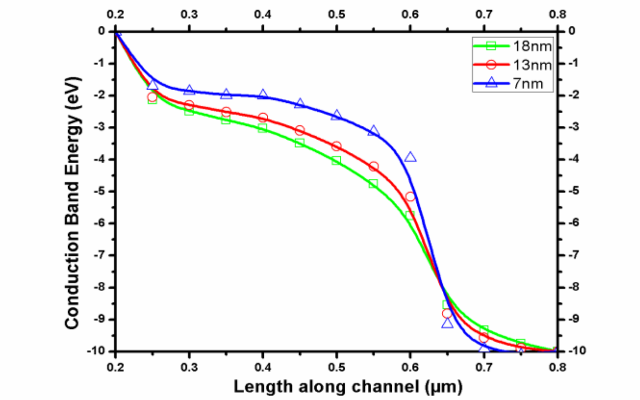

Fig. 7. Conduction Band Energy variation along the channel of U-DG InAlGaN/GaN HEMT for varying barrier widths at Vds = 10V and Vgs = 1 V (ON state).

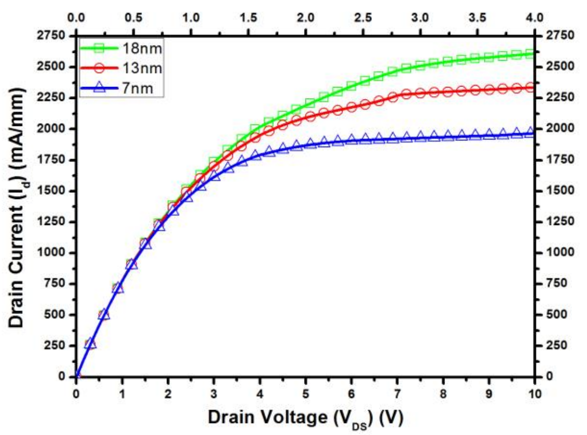

Fig. 8. Variation of I_d with V_{ds} of U-DG InAlGaN/GaN HEMT for varying barrier widths at V_{gs} = 1 V.

It has already been stated before that InAlGaN has a higher bandgap than AlGaN. Due to this large difference of conduction band energy between InAlGaN and GaN, InAlGaN/GaN structure experiences greater band bending. This results in deeper penetration of the GaN conduction band below the Fermi level at the heterojunction interface forming a stronger inversion channel layer than its ternary counterpart. Thus, it can be argued that charge density in the channel region being higher for quaternary HEMT, at a particular gate voltage, InAlGaN exhibits higher drain current (I_{ds}) variation with gate voltage (V_{gs}), compared to AlGaN/GaN MOS-HEMT, as depicted in **Fig.9**. Also for the same reason, greater negative voltage is required to undo the band bending, make the channel non-conducting and turn the device OFF, subsequently leading to lower threshold voltage in quaternary MOS-HEMT at V_{gs} = -8 V than the ternary one at V_{gs} = -3 V, as observed in **Fig.9**. If barrier depth, 'd' increases, then n_S(InAlGaN) also increases according to (8). This mathematical correspondence can also be validated theoretically, as greater amount of charge is bound to be stored in a thicker InAlGaN alloy layer.

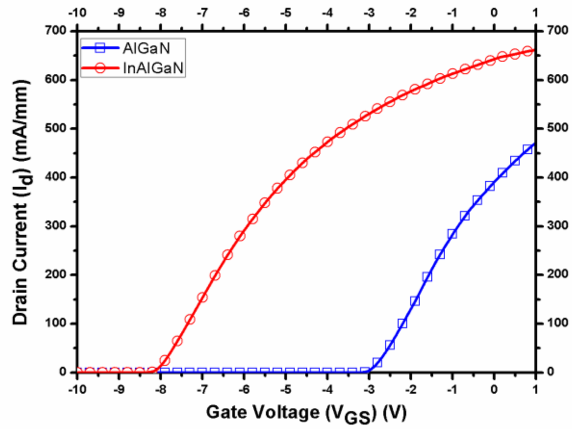

Fig. 9. Variation of I_d with V_{gs} of U-DG GaN HEMT for 18 nm InAlGaN and AlGaN barrier widths at V_{ds} = 1V.

Thus, InAlGaN/GaN based HEMT showcases higher drain current and lower threshold voltage values with gate voltage variation, appropriately viewed in **Fig.10**.

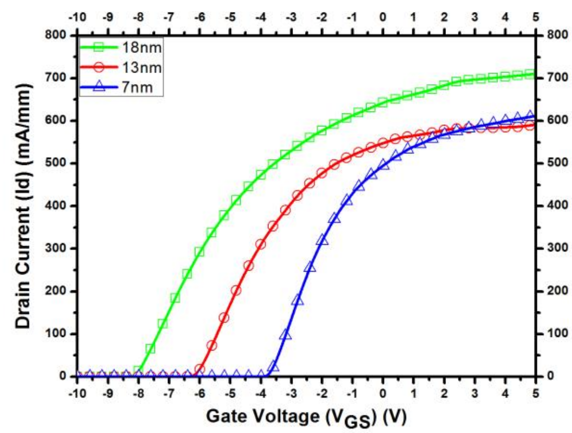

Fig. 10. Variation of I_d with V_{gs} of U-DG InAlGaN/GaN HEMT for varying barrier widths at V_{ds} = 1 V.

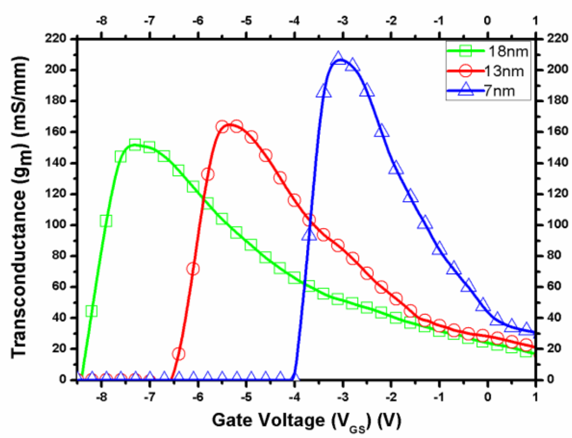

Fig. 11. Variation of g_m with V_{gs} of U-DG InAlGaN/GaN HEMT for varying barrier widths at V_{ds} = 1 V.

With decrease in InAlGaN width at same V_{gs}, magnitude of effective vertical electric field increases since,

$$E_{gs} = -\frac{\partial V_{gs}}{\partial r}\Big|_{V_{ds}=fixed} \qquad \ldots(9)$$

Thus, gate modulation capability increases which enhances device sensitivity and suppresses SCEs. As, device sensitivity is more, rate of change of I_d for small change in V_{gs} at a constant V_{ds} is more and that is why, the InAlGaN device with shortest barrier of 7 nm thickness exhibits a highest peak transconductance of 210 mS/mm, demonstrated in **Fig.11**.

Although, to establish gate control over lesser number of carriers in the channel, AlGaN/GaN MOS-HEMT with 18 nm barrier width has a higher $g_{m,max}$ of 190 mS/mm than the quaternary one with same width (170 mS/mm) **(Fig.12(b))**, the thinner barrier InAlGaN/GaN MOS-HEMT overtakes it, recording a peak transconductance of 210 mS/mm, depicted in **Fig.12(a)**.

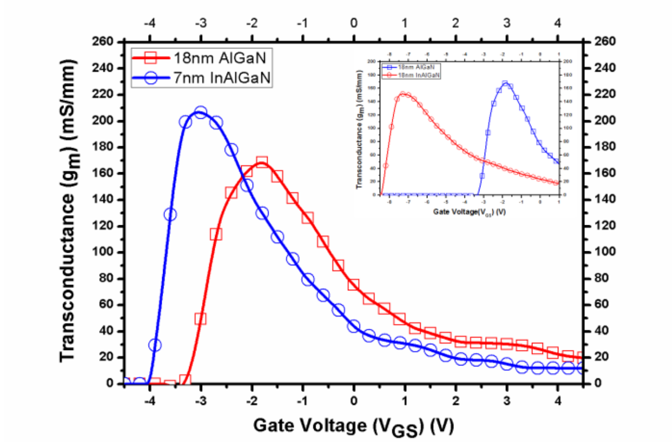

Fig. 12. (a) Variation of g_m as a function of V_{gs} of U-DG GaN HEMT for 18 nm AlGaN and 7 nm InAlGaN barrier widths at V_{ds} = 1V. (b) Inset: Variation of g_m as a function of V_{gs} of U-DG GaN HEMT for 18 nm AlGaN and InAlGaN barrier widths at V_{ds} = 1V.

Transconductance Generation Factor (TGF) relates the speed of the device with power dissipated as a function of gate voltage. High TGF value in the subthreshold region occurs due to the exponential dependence of drain current on gate voltage there and falls sharply afterwards as the device turns ON.

$$TGF = \frac{g_m}{I_d} = \frac{g_m r_o}{I_d r_o} = \frac{g_m r_o I_d}{V_{ds} I_d} = \frac{\text{Output Voltage}}{\text{Power Dissipated}} \qquad \ldots(10)$$

Devices with lower TGF before attaining threshold voltage provide better gain with smaller power dissipation, proving to be more efficient. From the above expression, it is clear that AlGaN having higher g_m value in subthreshold region with repect to InAlGaN of same barrier width will also have higher TGF, in line with **Fig.13**, and InAlGaN MOS-HEMTs with lower barrier width will have higher TGF for the same reason, as is evident from **Fig.14**.

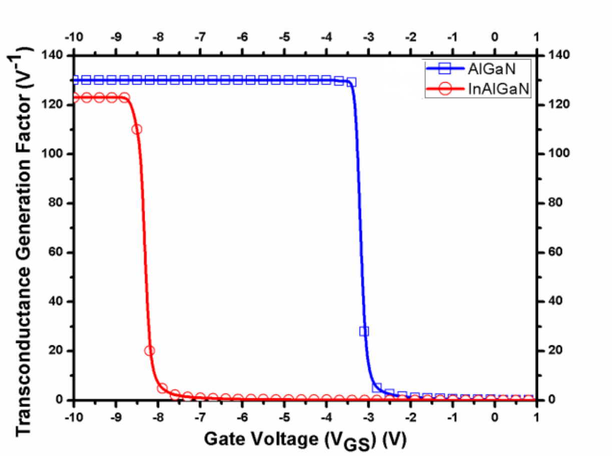

Fig. 13. Variation of Transconductance Generation Factor as a function of V_{gs} of U-DG GaN HEMT for 18 nm AlGaN and InAlGaN barrier widths at V_{ds} = 1 V.

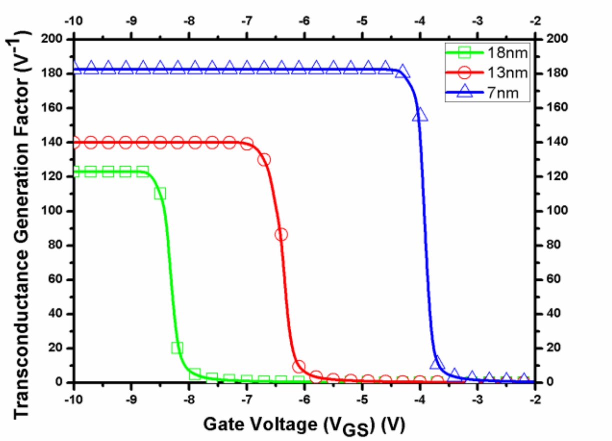

Fig. 14. Variation of Transconductance Generation Factor as a function of V_{gs} of U-DG InAlGaN/GaN HEMT for varying barrier widths at V_{ds} = 1 V.

Fig.15 demonstrates the average output resistances (r_o) for ternary AlGaN/GaN MOS-HEMT of 18 nm barrier width and quaternary InAlGaN/GaN MOS-HEMT for varying barrier widths of 18 nm, 13 nm and 7 nm over a range of V_{gs} values from -2 V to +0.5 V, keeping all devices in saturation. Since r_o is technically the slope of I_d-V_{ds} curve in saturation region, it is directly proportional to the absolute value of early voltage and inversely proportional to the saturation drain current in that region.

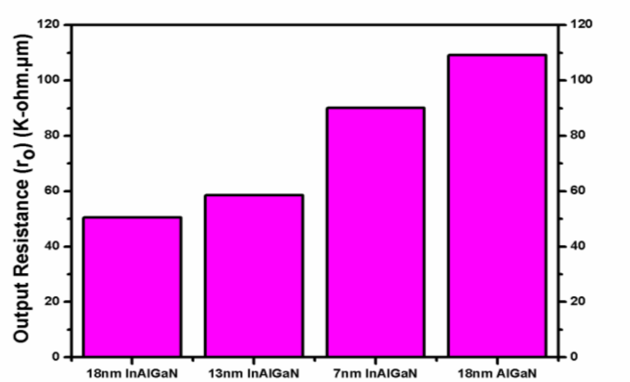

Fig. 15. Variation of average output resistances for varying barrier materials and widths over a range of V_{gs} values from -2 V to 0.5 V.

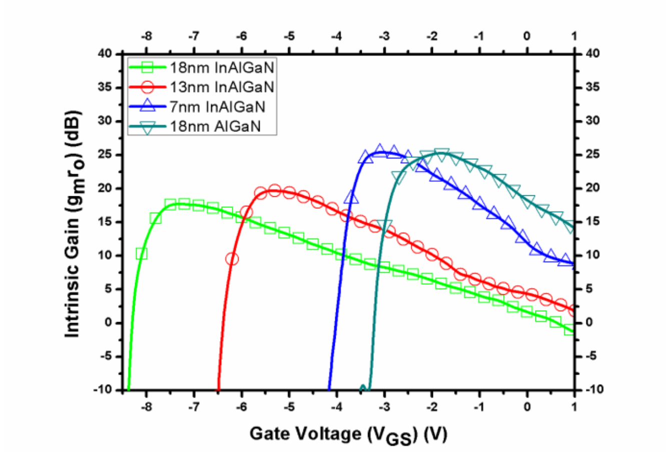

Fig. 16. Instrinsic Gain (in dB) variation as a function of V_{gs} for varying barrier materials and widths.

As discussed earlier, the I_{dsat} values for quaternary alloys are much more than that of ternary alloys, and as barrier height increases, increase in saturation drain values per unit change in V_{ds} at constant V_{gs} is more. Hence, $\frac{\partial Id}{\partial Vds}\big|_{Vgs\,=\,constant}$ in saturation region is more, thereby decreasing early voltage with increasing width. So, r_o is highest of value 90.09 KΩ.µm for least InAlGaN of width 7 nm among the three quaternary specimens and for ternary of value 109 KΩ.µm among all the four specimens, enlisted in Table.III. The intrinsic gain ($g_m r_o$) variation in dB of all the four devices with V_{gs} obtained by the product of transconductance (g_m) and output resistance (r_o) is appropriately exhibited in **Fig.16**.

TABLE III

Analog FoMs	$Al_{0.3}Ga_{0.7}N$/ GaN	$In_{0.05}Al_{0.75}Ga_{0.2}N$/ GaN	$In_{0.05}Al_{0.75}Ga_{0.2}N$ /GaN	$In_{0.05}Al_{0.75}Ga_{0.2}N$ /GaN
Barrier width	18 nm	18 nm	13 nm	7 nm
I_{dsat}	960 mA/mm	2610 mA/mm	2340 mA/mm	1960 mA/mm
V_{th}	-3 V	-8 V	-6 V	-4 V
$g_{m,max}$	168 mS/mm	151 mS/mm	164 mS/mm	207 mS/mm
TGF_{max}	130 V^{-1}	123 V^{-1}	140 V^{-1}	183 V^{-1}
r_o	109 KΩ.µm	50.46 KΩ.µm	58.6 KΩ.µm	90.09 KΩ.µm
$g_m r_{o,peak}$	25.3 dB	17.7 dB	19.7 dB	25.4 dB

IV. RF PERFORMANCE

The RF performance of an electronic device can be analyzed by drawing its small signal equivalent model, as depicted in **Fig.17**. Small signal equivalent circuits are extremely important for Analog and RF engineers to calculate the voltage gain, current gain, input impedance and output impedance at various operating frequencies. The small signal model consists of an intrinsic part, which includes parameters like gate-source capacitance (C_{gs}), gate-drain capacitance (C_{gd}), gate-source resistance (R_{gs}), gate-drain resistance (R_{gd}), dependent on external bias conditions and an extrinsic part, the parameters of which are independent of external bias. The RF FoMs that have been compared between the ternary AlGaN based MOS-HEMT and the quaternary InAlGaN based MOS-HEMT are the intrinsic gate capacitances, C_{gs}, C_{gd} and C_{gg}, cut-off frequency (f_T) and frequency of maximum oscillation (f_{MAX}).

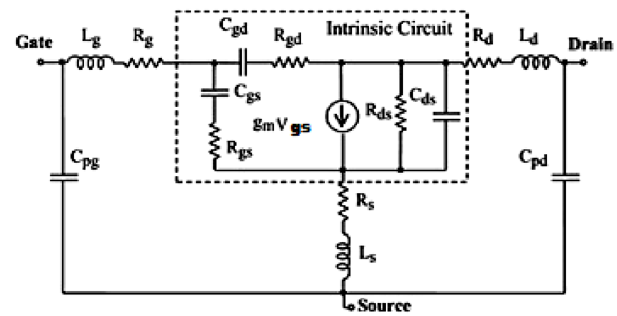

Fig. 17. Small Signal Model for an U-DG GaN based MOS-HEMT

The small signal parameters are obtained by computing the S parameters, i.e., the Y parameters and H parameters of the device. **Fig.18.** shows the variation of total gate capacitance (C_{gg}) with V_{gs} for quaternary and ternary GaN HEMTs at 100 GHz applied frequency. The nature of graph depicts that when channel is not sufficiently conducting in sub-threshold region, C_{gg} is mostly dominated by parasitic capacitances. In threshold region, large number of majority carriers starts accumulating in the channel, resulting in sharp increase in intrinsic capacitance (C_{gs} and C_{gd}) values. As the device approaches super threshold region, drain current is almost saturated and thus C_{gg} is constant at higher V_{gs}. The InAlGaN/GaN device having higher drain current has greater amount of charge stored per unit area in the channel and thus, exhibits greater intrinsic gate capacitance.

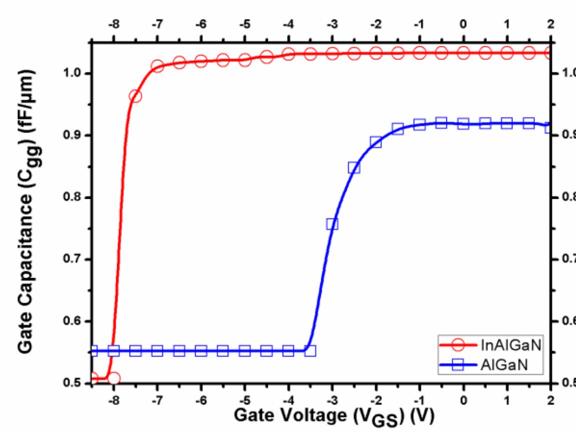

Fig. 18. Variation of C_{gg} with respect to V_{gs} of U-DG GaN HEMT for 18 nm AlGaN and InAlGaN barrier widths.

Maximizing f_T and f_{MAX} are primary goals for RF applications. f_T is the frequency at which current gain is unity and is an important parameter for high speed digital circuits.

On the other hand, f_{MAX} is the frequency at which power gain is unity and gives an indication of maximum available power gain, a realistic parameter for high frequency amplifiers **[31]**.

$$f_T = \frac{g_m}{2\Pi \cdot (C_{gs} + C_{gd})} \quad \ldots(11)$$

$$f_T = f_0 \cdot |H_{21}| \quad \ldots(12)$$

$$f_{MAX} = \frac{g_m}{2\Pi \cdot (C_{gs} + C_{gd}) \cdot \sqrt{4 \cdot (R_s + R_i + R_g) \cdot \left(g_{ds} + g_m \cdot \frac{C_{gd}}{C_{gs}} \right)}} \quad \ldots(13)$$

$$f_{MAX} = f_0 \cdot \sqrt{\frac{|Y_{21} - Y_{12}|^2}{4 \cdot \{\mathrm{Re}(Y_{11}) \cdot \mathrm{Re}(Y_{22}) - \mathrm{Re}(Y_{12}) \cdot \mathrm{Re}(Y_{21})\}}} \quad \ldots(14)$$

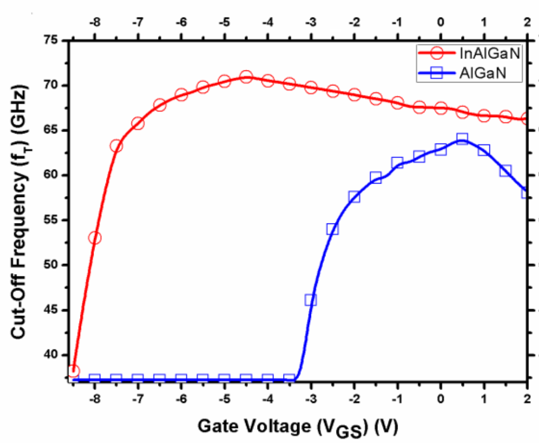

Fig. 19. Variation of cut-off frequency, f_T with respect to V_{gs} of U-DG GaN HEMT for 18 nm AlGaN and InAlGaN barrier widths.

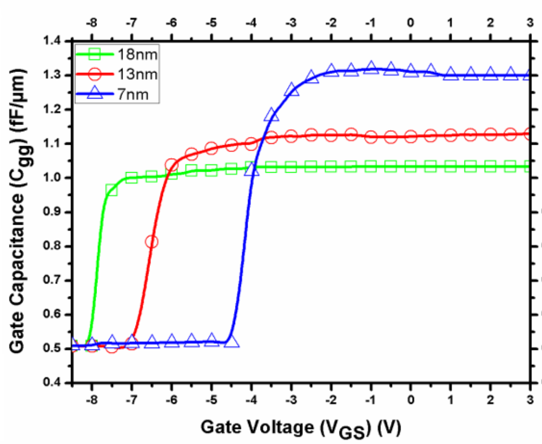

Fig. 20. Variation of C_{gg} with respect to V_{gs} of U-DG InAlGaN/GaN HEMT for varying barrier widths.

Fig.19 shows that quaternary InAlGaN HEMTs have higher maximum cut-off frequency of 71 GHz than ternary AlGaN HEMTs (64 GHz), the former thus more suitable for high speed applications. As barrier thickness rises, electrostatic control of the gate over the channel degrades and thus C_{gg} decreases, appropriately demonstrated in **Fig.20**. Increased width creates deeper triangular quantum well resulting in greater electron confinement within the well. As 2DEG concentration rises, drain current variation with V_{gs} also increases. Also, with increasing InAlGaN layer thickness, majority carriers move further away from the HfO_2-InAlGaN interface towards the InAlGaN-GaN interface reducing gate grip and thereby, g_m.

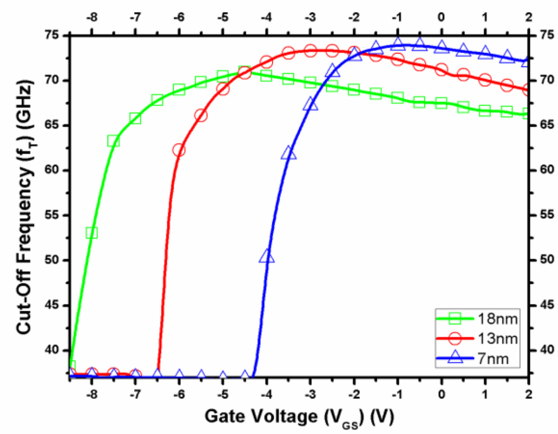

Fig. 21. Variation of cut-off frequency, f_T with respect to V_{gs} of U-DG InAlGaN/GaN HEMT for varying barrier widths.

Although, C_{gg} also decreases with increasing barrier depth, still rate of decrease of g_m is much more than that of former, and hence, highest f_T of 76 GHz is recorded for 7 nm InAlGaN/GaN MOS-HEMT, concluded from **Fig.21**.

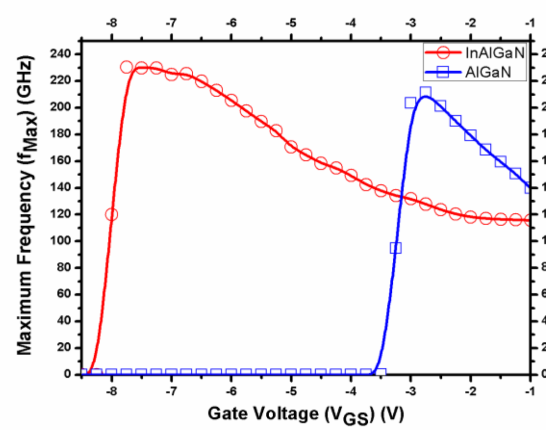

Fig. 22. Variation of f_{MAX} with respect to V_{gs} of U-DG GaN HEMT for 18 nm AlGaN and InAlGaN barrier widths.

Due to higher 2DEG concentration, the sheet resistance of InAlGaN/GaN structure is lower than that of AlGaN/GaN structure. This significantly reduced sheet resistance brings in low parasitic source and drain resistances, which contributes to enhancement of f_{MAX} values of the quaternary device with respect to the ternary one (**Fig.22**), establishing the former as a more worthy contestant for high frequency amplifiers. As the InAlGaN barrier becomes thinner, R_{gg} increases due to the decrease in the cross-section area and thus, f_{MAX} increases. Hence, 7 nm InAlGaN/GaN HEMT records highest peak f_{MAX} of 327 GHz, as evident from **Fig.23**.

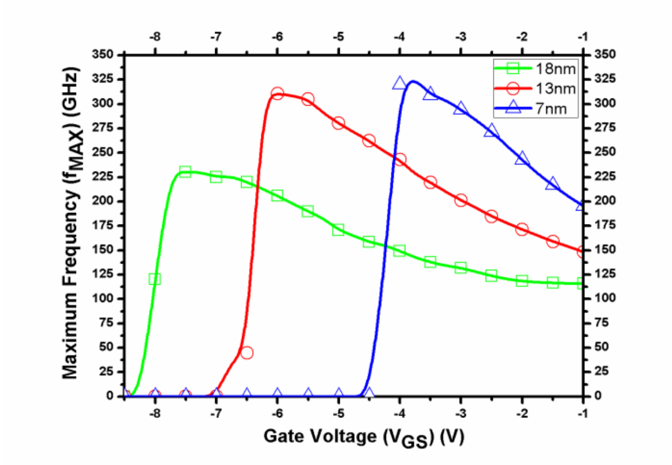

Fig. 23. Variation of f_{MAX} with respect to V_{gs} of U-DG InAlGaN/GaN HEMT for varying barrier widths.

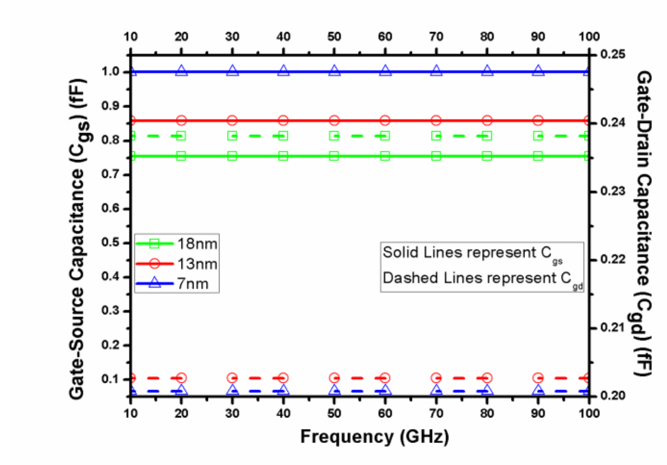

Fig. 25. Variation of C_{gs} and C_{gd} as a function of frequency of U-DG InAlGaN/GaN HEMT for varying barrier widths.

The intrinsic capacitance values with applied frequency varying from 10 GHz to 100 GHz for InAlGaN MOS-HEMT and AlGaN MOS-HEMT of same barrier width, 18 nm and by varying three different InAlGaN thicknesses i.e. 18 nm, 13 nm and 7 nm are plotted in **Fig.24** and **Fig.25** respectively, and are listed in Table.IV. The C_{gs} and C_{gd} values for all the 4 models are simulated at their respective thresholds where g_m attains its peak. As the device attains saturation, drain current flowing from drain to source causes more charge carriers to migrate from the source end and accumulate at the drain end, thereby decreasing source-side capacitance, C_{gs} and increasing drain-side capacitance, C_{gd} by the same magnitude, eventually keeping the total charge in the channel constant. Therefore, as in **Fig.25,** C_{gs} is highest and C_{gd} is lowest for 7 nm InAlGaN, while C_{gs} is lowest and C_{gd} is highest 18 nm InAlGaN.

TABLE IV

RF parameters	**$Al_{0.3}Ga_{0.8}N$/ GaN**	**$In_{0.05}Al_{0.75}Ga_{0.2}N$ /GaN**	**$In_{0.05}Al_{0.75}Ga_{0.2}N$ /GaN**	**$In_{0.05}Al_{0.75}Ga_{0.2}N$ /GaN**
Barrier width	18nm	18nm	13nm	7nm
$f_{T,peak}$	64.049 GHz	70.950 GHz	73.346 GHz	75.769 GHz
$f_{MAX,peak}$	211.238 GHz	230.488 GHz	313.921 GHz	326.703 GHz
C_{gs}	0.745 fF	0.755 fF	0.859 fF	1.00 fF
C_{gd}	0.214 fF	0.238 fF	0.203 fF	0.201 fF

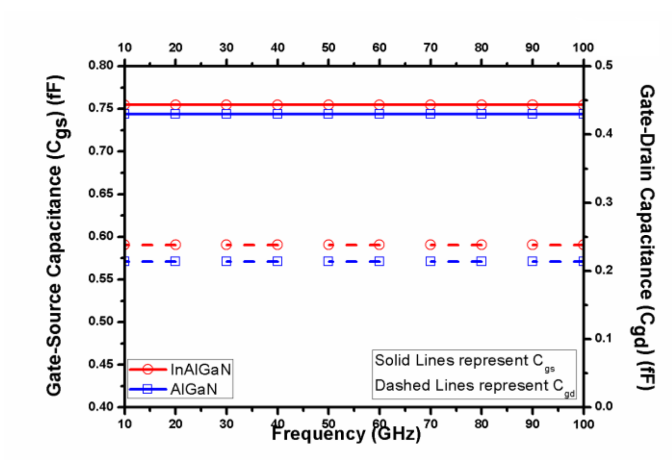

Fig. 24. Variation of C_{gs} and C_{gd} as a function of frequency of U-DG GaN HEMT for 18 nm AlGaN and InAlGaN barrier widths.

V. Large Signal Analysis

Large signal measurements has been performed on all the devices at an applied frequency of 100 GHz for input signal strength varying from 30 dBm to 50 dBm, as labelled in **Fig.26**, **Fig.27** and **Fig.28**. The parameters computed to analyze the power performance of each device are Gain, Output Power (P_{out}) and Power Output Efficiency (POE), as listed in Table.V.

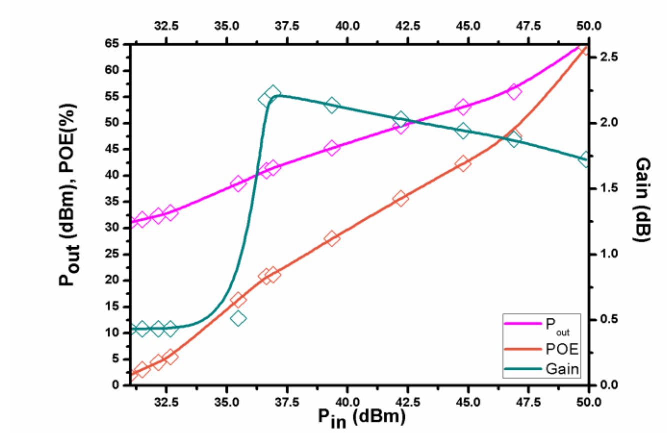

Fig. 26. Variation of P_{out}, POE and Gain with P_{in} of U-DG AlGaN/GaN MOS-HEMT with 18 nm barrier width.

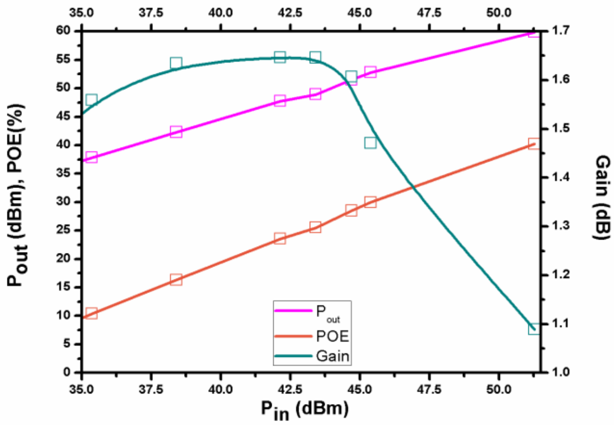

Fig. 27. Variation of P_{out}, POE and Gain with P_{in} of U-DG InAlGaN/GaN MOS-HEMT with 18 nm barrier width.

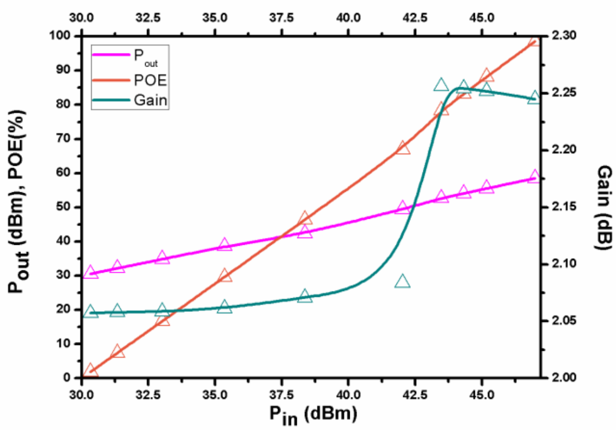

Fig. 28. Variation of P_{out}, POE and Gain with P_{in} of U-DG InAlGaN/GaN MOS-HEMT with 7 nm barrier width.

From the graphs, it is clear that P_{out} and POE grows almost linearly with P_{in}, but the gain attains its peak at a particular input signal power and thereafter decays. From Table.5, it is conclusive that though peak gain, output power density and efficiency for a particular input signal power is more for ternary alloy MOS-HEMT than quaternary alloy MOS-HEMT of same alloy width, i.e. 18 nm, thinning the quaternary InAlGaN barrier contributes to even higher peak gain, P_{out} and POE, thus providing better power performance. Thus, the highest peak gain, 2.256 dB with an output power of 55 dBm and efficiency 87.5 % at 45 dBm input power is recorded for the 7 nm InAlGaN/GaN MOS-HEMT.

TABLE V

Power Performance parameters	**$Al_{0.3}Ga_{0.8}N$/ GaN**	**$In_{0.05}Al_{0.75}Ga_{0.2}N$/ GaN**	**$In_{0.05}Al_{0.75}Ga_{0.2}N$/ GaN**
Barrier width	18nm	18nm	7nm
Peak Gain	2.23 dB	1.65 dB	2.26 dB
P_{out} at P_{in} = 45 dBm	53 dBm	52 dBm	55 dBm
POE at P_{in} = 45 dBm	42.5 %	29 %	87.5 %

VI. Conclusion

A comparison has been drawn between some of the important performance parameters of this device and those of a similar fabricated device [15] and presented in Table.VI.

TABLE VI

Parameters		**Ref. 15**	**This work**
		Single T-shaped Gate $In_{0.05}Al_{0.75}Ga_{0.2}N$/GaN/AlN HEMT having 7 nm InAlGaN barrier width with 1nm AlN interlayer	Underlapped Double Gate $In_{0.05}Al_{0.75}Ga_{0.2}N$/GaN MOS-HEMT having 7 nm InAlGaN barrier width
Analog	2DEG concentration	$2 \times 10^{13} cm^{-2}$	$1.789 \times 10^{13} cm^{-2}$
	I_{dsat}	1.94 A/mm at V_{gs}=2V	1.96 A/mm at V_{gs}=1V
	V_{th}	- 4.5 V	- 4 V
	$g_{m,peak}$	506 mS/mm at V_{ds} = 10 V	207 mS/mm at V_{ds} = 1 V
RF	$f_{T,peak}$	142 GHz	75.769 GHz
	$f_{MAX,peak}$	203 GHz	326.703 GHz
Power	Efficiency	33.6 %	87.5 %
	Gain	7.88 dB	2.26 dB

Development of InAlGaN/GaN MOS-HEMT with special focus on the quaternary InAlGaN layer has resulted in substantial performance improvement. Owing to the significant rise in the 2DEG density, the saturation drain current density records to 2610 mA/mm at V_{gs} = 1 V compared to 960 mA/mm of its ternary counterpart with same barrier width of 18 nm. The peak f_T and f_{MAX} values for 18 nm AlGaN HEMT are recorded as 64 GHz and 211 GHz respectively, while those for InAlGaN HEMT becomes 71 GHz and 230 GHz having same barrier thickness, which rises to as high as 76 GHz and 327 GHz for 7 nm InAlGaN width, thereby establishing quaternary MOS-HEMT as a more promising alternative for high frequency RF applications. Moreover, 7 nm InAlGaN barrier also provides a $g_{m,max}$ of 210 mS/mm at V_{ds} = 1 V, this is 10.5 % greater than that of 18 nm AlGaN HEMT, which is 190 mS/mm. This sizeable increased transconductance and reduced parasitic capacitances and resistances validate the use of thinner barrier InAlGaN/GaN MOS-HEMTs for high sensitive and low power circuits. Enhanced output power efficiency for the 7 nm InAlGaN HEMT, which is more than twice of that of 18 nm AlGaN HEMT at 45 dBm input power, establishes lower barrier width quaternary MOS-HEMT as a suitable candidate for high power applications.

Acknowledgment

The authors are thankful to the IEEE EDS Center of Excellence, Heritage Institute of Technology, Kolkata, for providing necessary laboratory facilities.

References

[1] T. Palacios, C. Suh, A. Chakraborty, S. Keller, S. P. DenBaars and U. K. Mishra, "High-performance E-mode AlGaN/GaN HEMTs," in *IEEE Electron Device Letters*, vol. 27, no. 6, pp. 428-430, June 2006, DOI: 10.1109/LED.2006.874761.

[2] I. P. Smorchkova, C. R. Elsass, J. P. Ibbetson, R. Vetury, B. Heying et al., "Polarization-induced charge and electron mobility in AlGaN/GaN heterostructures grown by plasma-assisted molecular-beam epitaxy", *J. Appl. Phys.*, vol. 86, no. 8, pp. 4250-4526, Oct. 1999, DOI: 10.1063/1.371396.

[3] U. K. Mishra, L. Shen, T. E. Kazior and Y. Wu, "GaN-based RF power devices and amplifiers," in *Proceedings of the IEEE*, vol. 96, no. 2, pp. 287-305, Feb. 2008, DOI: 10.1109/JPROC.2007.911060.

[4] S. Baskaran, A. Mohanbabu, N. Anbuselvan, N. Mohankumar, D. Godwinraj, and C.K. Sarkar, "Modeling of 2DEG sheet carrier density and DC characteristics in spacer based AlGaN/AlN/GaN HEMT devices", *Superlattices and Microstructures*, vol. 64, pp. 470-482, Oct. 2013, DOI: 10.1016/j.spmi.2013.10.019.

[5] H. Mukherjee, R. Dasgupta, M. Kar and A. Kundu, "A comparative analysis of analog performances of underlapped dual gate AlGaN/GaN based MOS-HEMT and Schottky-HEMT," *2020 IEEE Calcutta Conference (CALCON)*, Kolkata, India, 2020, pp. 412-416, DOI: 10.1109/CALCON49167.2020.9106420.

[6] Z. Touati, Z. Hamaizia and Z. Messai, "DC and RF characteristics of AlGaN/GaN HEMT and MOS-HEMT," *2015 4th International Conference on Electrical Engineering (ICEE)*, Boumerdes, 2015, pp. 1-4, DOI: 10.1109/INTEE.2015.7416850.

[7] C. Ma, and Z. Gu, "Review of GaN HEMT Applications in Power Converters over 500 W", in *Electronics*, vol. 8, no. (12)1401, pp. 1-29, Nov. 2019, DOI: 10.3390/electronics8121401.

[8] J. Hwang, W. J. Schaff, L. F. Eastman, S. T. Bradley, L. J. Brillson, D. C. Look, J. Wu, W. Walukiewicz, M. Furis, and A. N. Cartwright, "Si doping of high-Al-mole fraction Al x Ga 1−x N alloys with rf plasma-induced molecular-beam-epitaxy", *Applied Physics Letters*, vol. 81, no. 27, pp. 5192-5194, 2002, DOI: 10.1063/1.1534395.

[9] S. Einfeldt *et al.*, "Strain relaxation in AlGaN under tensile plane stress", *J. Appl. Phys.*, vol. 88, no. 12, pp. 7029–7036, Dec. 2000, DOI: 10.1063/1.1326852.

[10] R. Butt´e, J. F. Carlin, E. Feltin, M. Gonschorek, S. Nicolay, G. Christmann, D. Simeonov, A. Castiglia, J. Dorsaz, H. J. Buehlmann, S. Christopoulos, G. Baldassarri H¨oger von H¨ogersthal, A. J. D. Grundy, M. Mosca, C. Pinquier, M. A. Py, F. Demangeot, J. Frandon, P. G. Lagoudakis, J. J. Baumberg and N. Grandjean, "Current status of AlInN layers lattice-matched to GaN for photonics and electronics", *J. Phys. D: Appl. Phys.*, vol. 40, no. 20, Jun. 2007, pp. 6328-6344, DOI: 10.1088/0022-3727/40/20/S16.

[11] Z. L. Miao *et al.*, "Magnetotransport properties of lattice-matched $In_{0.18}Al_{0.82}N$/AlN/GaN heterostructures," *J. Appl. Phys.*, vol. 109, no. 1, Art. no. 016102, pp. 1-3, Jan. 2011, DOI: 10.1063/1.3525989.

[12] R. D. Quan *et al.*, "Fabrication of InAlGaN/GaN high electron mobility transistors on sapphire substrates by pulsed metal organic chemical vapor deposition," *Chin. Phys. Lett.*, vol. 33, no. 10, Art. no. 108104, pp. 1-4, Jun. 2016, DOI: 10.1088/0256-307X/33/10/108104.

[13] S. Sahu, M. Mohapatra, A.K. Panda, "DC and RF performance evaluation of nano-scale InAlGaN/GaN HEMT", *International Journal of Scientific and Engineering Research*, vol. 5, issue 5, pp. 6-10, May. 2018.

[14] M. A. Abid, H. A. Hassan, Z. Hassan, S. S. Ng, N. H. Abd. Raof et al., "The study of energy band gap of $Al_xIn_yGa_{1-x-y}N$ quaternary alloys using UVVIS spectroscopy", *AIP Conf. Proc.*, vol. 1250, pp. 297-300, 2010, DOI: 10.1063/1.3469662.

[15] W. Wang, X. Yu, J. Zhou, D. Chen, K. Zhang, C. Kong, Y. Kong, Z. Li, and T. Chen, "Improvement of power performance of GaN HEMT by using quaternary InAlGaN barrier", *Journal of the Electron Devices Society*, vol. 6, Feb. 2018, pp. 360-364, DOI: 10.1109/JEDS.2018.2807185.

[16] F. Lecourt, A. Agboton, N. Ketteniss, H. Behmenburg, N. Defrance, V. Hoel, H. Kalisch, A. Vescan, M. Heuken, and J. De Jaeger, "Power Performance at 40 GHz on Quaternary Barrier InAlGaN/GaN HEMT", *IEEE Electron Device Letters*, vol. 34, no. 8, pp. 978-980, Aug. 2013.

[17] T. Lim, R. Aidam, L. Kirste, P. Waltereit, R. Quay, S. Müller, and O. Ambacher, "Compositional variation of nearly lattice-matched InAlGaN alloys for high electron mobility transistors", *Applied Physics Letters*, vol. 96, no. 25, Art. no. 252108, pp. 1-3, Jun. 2010, DOI: 10.1063/1.3456561.

[18] N. Ketteniss, L. R. Khoshroo, M. Eickelkamp, M. Heuken, H. Kalisch, R. H. Jansen and A. Vescan, "Study on quaternary AlInGaN/GaN HFETs grown on sapphire substrates", *Semicond. Sci. Technol.*, vol. 25, no. 7, Art. No. 075013, pp. 1-5, Jun. 2010, DOI: 10.1088/0268-1242/25/7/075013.

[19] F. Lecourt, Y. Douvry, N. Defrance, V. Hoel, J.C. De Jaeger, S. Bouzid, M. Renvoise, D. Smith and H. Maher, " High transconductance AlGaN/GaN HEMT with thin barrier on Si(111) substrate", in *2010 Proc. ESSDERC*, Sevilla, Spain, 2010, pp. 281-284, DOI: 10.1109/ESSDERC.2010.5618362.

[20] M. Higashiwaki, Y. Pei, R. Chu, and U. K. Mishra, "Effects of barrier thinning on small-signal and 30-GHz power characteristics of AlGaN/GaN Heterostructure Field-Effect Transistors", *IEEE Transactions on Electron Devices*, vol. 58, no. 6, pp. 1681-1686, Jun. 2011, DOI: 10.1109/TED.2011.2131653.

[21] A.G. Gudkov et al., "The Influence of AlGaN Barrier-Layer Thickness on the GaN HEMT Parameters for Space Applications", in Anisimov K. et al. (eds), *Proceedings of the Scientific-Practical Conference "Research and Development – 2016"*, Springer, Cham, Switzerland, 2017, pp. 273-280, DOI: 10.1007/978-3-319-62870-7_30.

[22] P. Waltereit, W. Bronner, M. Musser, F. van Raay, M. Dammann, M. Casar, S. Müller, L. Kirste, K. Kohler, R. Quay, M. Mikulla, and O. Ambacher, "Influence of AlGaN barrier thickness on electrical and device properties in $Al_{0.14}Ga_{0.86}N$/GaN High Electron Mobility Transistor Structures", *Journal of Applied Physics*, vol. 112, no. 5, Art. no. 053718, pp. 1-5, Sep. 2012, DOI: 10.1063/1.4752257.

[23] H. Pardeshi, “Analog/RF performance of AlInN/GaN underlap DG MOS-HEMT”, *Superlattice and Microstructures*, vol. 88, pp. 508–517, Oct. 2015, DOI: 10.1016/j.spmi.2015.10.009.

[24] A. Kundu, A. Dasgupta, R. Das, S. Chakraborty, A. Dutta, C. K. Sarkar, “Influence of underlap on gate stack DG-MOSFET for analytical study of Analog/RF performance”, *Superlattice and Microstructures*, vol. 94, pp. 60–73, Jun. 2016, DOI: 10.1016/j.spmi.2016.04.013.

[25] A. Mondal, A. Roy, R. Mitra, and A. Kundu, “Comparative study of variations in gate oxide material of a novel underlap DG MOS-HEMT for Analog/RF and high power applications”, Silicon, vol. 12, pp. 2251–2257, 2020, DOI: 10.1007/s12633-019-00316-0.

[26] K. P. Pradhan, S. K. Mohapatra, P. K. Sahu, D. K. Behara, “Impact of high-k gate dielectric on analog and RF performance of nanoscale DG-MOSFET”, *Microelectronics Journal*, vol. 45, issue 2, pp. 144-151, Feb. 2014, DOI: 10.1016/j.mejo.2013.11.016.

[27] T. R. Lenka, A. K. Panda, “AlGaN/GaN-based HEMT on SiC substrate for microwave characteristics using different passivation layers”, *Pramana – J. Phys.*, vol. 79, no. 1, pp. 151-163, Jul. 2012, DOI: 10.1007/s12043-012-0290-9.

[28] A. Roy, R. Mitra and A. Kundu, "Influence of Channel Thickness on Analog and RF Performance Enhancement of an Underlap DG AlGaN/GaN based MOS-HEMT Device," *2019 Devices for Integrated Circuit (DevIC)*, Kalyani, India, 2019, pp. 186-190, DOI: 10.1109/DEVIC.2019.8783865.

[29] M. Allaei, M. Shalchian and F. Jazaeri, "Modeling of short-channel effects in GaN HEMTs," in *IEEE Transactions on Electron Devices*, vol. 67, no. 8, pp. 3088-3094, Aug. 2020, DOI: 10.1109/TED.2020.3005122.

[30] Y. U. Tarauni, D. J. Thiruvadigal, H. B. Joseph, “Characterization and optimization of MIS-HEMTs device of high-kdielectric material on quaternary barrier of $Al_{0.42}ln_{0.03}Ga_{0.55}N$/UID-AIN/GaN/GaN heterostructure for high power switching application”, *Applied Surface Science*, vol. 488, pp. 427-433, May. 2019, DOI: 10.1016/j.apsusc.2019.05.170.

[31] Y. Tang *et al.*, "Ultrahigh-speed GaN High-Electron-Mobility Transistors with f_T/f_{MAX} of 454/444 GHz," in *IEEE Electron Device Letters*, vol. 36, no. 6, pp. 549-551, June 2015, DOI: 10.1109/LED.2015.2421311.

Conflicts of Interest Statement

Manuscript title:

Enhancement in Analog/RF and Power Performance of Underlapped DG Quaternary InAlGaN/GaN MOSHEMTs

The authors whose names are listed immediately below certify that they have NO affiliations with or involvement in any organization or entity with any financial interest (such as honoraria; educational grants; participation in speakers' bureaus; membership, employment, consultancies, stock ownership, or other equity interest; and expert testimony or patent-licensing arrangements), or non-financial interest (such as personal or professional relationships, affiliations, knowledge or beliefs) in the subject matter or materials discussed in this manuscript.

Author names:

The authors whose names are listed immediately below report the following details of affiliation or involvement in an organization or entity with a financial or non-financial interest in the subject matter or materials discussed in this manuscript. Please specify the nature of the conflict on a separate sheet of paper if the space below is inadequate.

Author names:

1. **Hrit Mukherjee**
   Department of Electronics and Telecommunication Engineering,
   Jadavpur University, Kolkata, India.
   Email: hritmukherjee@gmail.com

2. **Mousiki Kar**
   Department of Electronics and Communications Engineering,
   Heritage Institute of Technology, Kolkata, India.
   Email: mousikikar@gmail.com

3. **Atanu Kundu**
   Department of Electronics and Communications Engineering,
   Heritage Institute of Technology, Kolkata, India.
   Email: kundu.atanu@gmail.com

This statement is signed by all the authors to indicate agreement that the above information is true and correct (*a photocopy of this form may be used if there are more than 10 authors*):

Author's name (typed)	Author's signature	Date
Hrit Mukherjee	Hrit Mukherjee	10/09/2020
Mousiki Kar	Mousiki Kar	10/09/2020
Atanu Kundu	Atanu Kundu	10/09/2020